Semiconducting Graphene on Silicon from First-Principles Calculations

Xuejie Dang,† Huilong Dong,† Lu Wang, Yanfei Zhao, Zhenyu Guo, Tingjun Hou, Youyong Li,* and Shuit-Tong Lee*

Institute of Functional Nano & Soft Materials (FUNSOM), Soochow University, Suzhou 215123, China. †X. Dang and H. Dong contributed equally.

ABSTRACT Graphene is a semimetal with zero band gap, which makes it impossible to turn electric conduction off below a certain limit. Transformation of graphene into a semiconductor has attracted wide attention. Owing to compatibility with Si technology, graphene adsorbed on a Si substrate is particularly attractive for future applications. However, to date there is little theoretical work on band gap engineering in graphene and its integration with Si technology. Employing first-principles calculations, we study the electronic properties of monolayer and bilayer graphene adsorbed on clean and hydrogen (H)-passivated Si (111)/Si (100) surfaces. Our calculation shows that the interaction between monolayer graphene and a H-passivated Si surface is weak, with the band gap remaining negligible. For bilayer graphene adsorbed onto a H-passivated Si surface, the band gap opens up to 108 meV owing to asymmetry introduction. In contrast, the interaction between graphene and a clean Si surface is strong, leading to formation of chemical bonds and a large band gap of 272 meV. Our results provide guidance for device designs based on integrating graphene with Si technology.

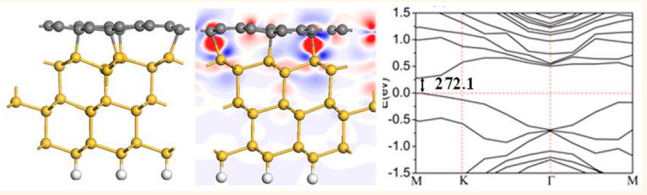

KEYWORDS: graphene · silicon · band gap · graphene–Si interaction

The zero band gap of graphene makes it impossible to turn off electrical conduction below a certain limit.[1] Band gap widening of graphene has thus attracted wide attention, because a sizable band gap can vastly enhance the potential of graphene in various applications.[2] The electronic properties of graphene can be modified by the application of magnetic and electric fields, molecule or atom adsorptions, interactions with substrates, and geometry control and chemical doping in graphene.[3−15] Major chip makers are actively pursuing graphene research, as the International Technology Roadmap for Semiconductors widely considers graphene as a promising candidate material for post-silicon electronics.

There are two practical routes to obtain a band gap in graphene. One route is to fabricate the graphene sheet into nanoribbons (to produce a band gap >100 meV).[16−20] Another route is to break the equivalence between sublattices by putting graphene on a substrate.[5,21−24] Various remarkable electronic properties of graphene have been achieved *via* substrate-induced perturbations. Different materials, including SiC,[25−28] BN,[29−31] SiO_2,[32−34] and metals,[7,35−38] have been successfully used as the substrates. Based on DFT calculation results, the band gap of graphene was obtained at 260 meV on SiC,[28] 53 meV on h-BN,[29] and 15 meV on a SiO_2 (0001) surface,[34] respectively. Besides single-layered graphene, the band gap modulation on bilayer graphene is also reported. Ohta *et al.*[39] first reported the synthesis of bilayer graphene by depositing it on insulating silicon carbide and tried to control the band gap of bilayer graphene by controlling the carrier density. Zhang *et al.*[40] obtained a gate-controlled, continuously tunable band gap of up to 250 meV by applying a variable external electric field. Similar work on the tunable band gap of bilayer graphene caused by the electric field effect was also reported by Castro *et al.*[41]

Silicon is the dominant material in the semiconductor industry. For its compatibility with Si technology, graphene adsorbed on a Si substrate may be a promising substitute for future applications. Hackley *et al.*[42] used solid source molecular beam epitaxy to grow graphitic carbon on Si(111). Xu *et al.*[43] performed experiments and *ab initio* calculations to study the electronic properties of

* Address correspondence to apannale@suda.edu.cn, yyli@suda.edu.cn.

Received for review June 18, 2015 and accepted July 27, 2015.

Published online July 27, 2015
10.1021/acsnano.5b03722

graphene deposited on clean and hydrogen (H)-passivated silicon (100) substrates. They found that a Si (100)/H surface does not perturb the electronic properties of graphene, whereas the interaction between the clean Si (100) surface and graphene changes the electronic states of graphene significantly. J. S. Moon *et al.*[44] reported top-gated graphene-on-Si n-FETs and p-FETs on 75 mm diameter Si (111) substrates showing clear ambipolar characteristics. Based on *ab initio* calculations, Tayran *et al.*[45] found that the graphene layer formed strong bonds with bare Si and a wavy structure *via* covalent bonding to Si.

Experimental studies[42,43] revealed promising applications of graphene adsorbed on a Si substrate. However, theoretical studies are necessary to illustrate the interaction modes between graphene and a Si substrate to design applications. Previous theoretical studies provided only relatively limited information for the interaction between graphene and Si (100)[43] or Si (111).[45] Here, we perform a systematic and detailed density functional theory (DFT) study of monolayer and bilayer graphene adsorbed on clean and H-passivated Si (111)/Si (100) surfaces in all possible configurations.

We find that the H-terminated Si (111)/H or (100)/H surface does not affect the electronic properties of the adsorbed graphene. In contrast, interactions between a clean Si (111) or Si (100) substrate and graphene change the electronic properties of graphene significantly. The resulting nonequivalence of the two carbon sites leads to opening of band gaps as high as 272 meV in monolayer graphene at the Dirac points. For bilayer graphene, the upper layer keeps the "perfect" plain structure and the unique physical properties of graphene, with a finite band gap of 108 meV, whereas the lower layer shows no graphitic electronic properties but acts as a buffer layer (BL) between the substrate and subsequent graphene layers.

RESULTS AND DISCUSSION

Monolayer Graphene on a Si Surface. We construct the structures of monolayer graphene on a Si surface according to the three configurations "T", "B", and "H", as shown in Figure S1 in the Supporting Information. The initial distance between graphene and the topmost layer of the Si surface was set to 2.5 Å for both hydrogenated Si and clean Si, which is the typical van der Waals interaction distance. Detailed modeling and structural information can be found in the Supporting Information.

After full geometry optimization, we find no covalent bonding between C and Si atoms for Si surface passivated by hydrogen atoms (Figure 1a–d). For a clean Si surface, the graphene layer is attached to Si forming Si–C σ covalent bonds (Figure 1e–h). For a Si(111) surface, the Si–C bond lengths range from 2.06 to 2.18 Å (B), 2.06 to 2.19 Å (H), and 2.04 to 2.10 Å (T), respectively. For a Si (100) surface, the Si–C bond lengths range from 2.06 to 2.07 Å. The Si–C bonds are slightly longer than the SiC bond length (1.92 Å), indicating there is strain energy in forming Si–C bonds between graphene and Si.

In Table 1, we summarize the adsorption energies of a graphene monolayer on Si surfaces. The adsorption energies are calculated according to

$$\Delta E = E_{\text{graphene/Si}} - (E_{\text{graphene}} + E_{\text{Si}})$$

where $E_{\text{graphene/Si}}$ is the total energy of the hybrid system, E_{graphene} is the energy of the isolated graphene, and E_{Si} is the energy of the relaxed Si substrate.

Since graphene forms chemical bonds with a clean Si surface, the adsorption energy of graphene on a clean Si surface is higher than that on a hydrogenated Si surface. By the same token, the average distance between graphene and a clean Si surface is shorter than that between graphene and a hydrogenated Si surface.

From Table 1, the adsorption energies and the average distances indicate that graphene interacts stronger with a Si (111) surface than a Si (100) surface. In graphene/Si (111) hybrid systems, four Si–C bonds are formed among 18 C atoms, whereas only eight Si–C bonds formed among 84 C atoms in a graphene/Si (100) hybrid system.

For the Si (111) surface, we consider three possible configurations, T, B, and H, as shown in Figure S1. As summarized in Table 1 and Figure 1, although the three configurations show similar distance and adsorption energy, they show quite different band gaps.

In Figure 1, we summarize the results for monolayer graphene on different silicon surfaces. As expected, the linear bands near the Dirac point of pristine monolayer graphene are maintained on the hydrogenated Si surfaces (see Figure 1a–d), due to the weak interaction between graphene and the Si substrate. Since there is no charge transfer between the graphene and Si substrate, the Fermi level lies at the Dirac point.

However, focusing on the bands near the Fermi levels shows that the π and π^* bands repel each other, forming finite energy gaps at the Dirac points, 0, 20, 18, and 108.8 meV for ghsi111_T, ghsi111_B, ghsi111_H, and ghsi100, respectively. Thus, the graphene adsorbed on the hydrogenated Si surface is no longer metallic with massless electrons, but becomes semiconducting with a direct narrow gap except for ghsi111_T. Indeed, the different band gaps reflect the asymmetry introduced to graphene upon adsorption on the Si surface. For ghsi111_T, the carbon atoms of graphene are on top of the Si atoms of the Si surface, and the symmetry is unchanged. Thus, the band gap of graphene remains zero. For ghsi111_B and ghsi111_H, as the carbon atoms of graphene are not on top of Si atoms of the Si surface, the symmetry is changed and the band gap is open. The structures of T, B, and H can be found in Figure S1. For ghsi100, since the Si (100)

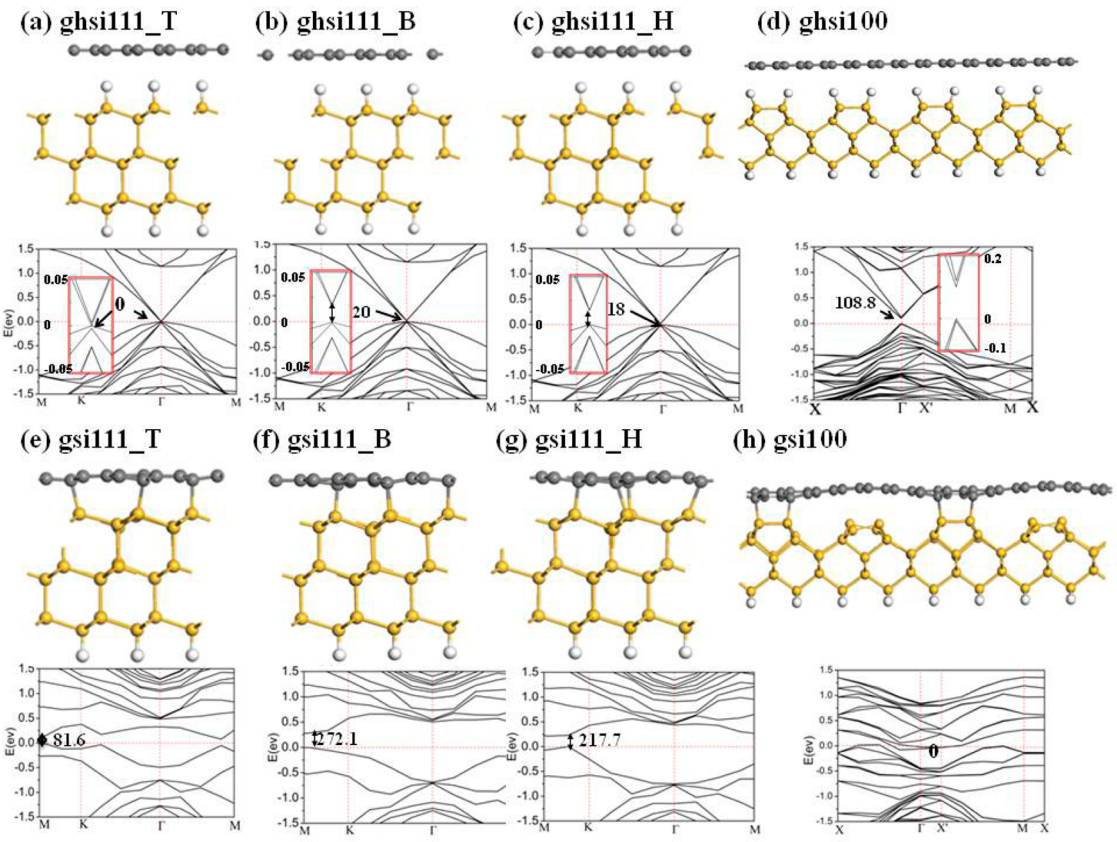

Figure 1. Monolayer graphene on different silicon surfaces and the corresponding band structures. (a) ghsi111_T, (b) ghsi111_B, (c) ghsi111_H, (d) ghsi100, (e) gsi111_T, (f) gsi111_B, (g) gsi111_H, and (h) gsi100. "ghsi111_T" represents graphene-hydrogen-silicon-111 surface with T configuration. The definition of T configuration, B configuration, and H configuration can be found in Figure S1 in the Supporting Information. Ghsi111_T, ghsi111_B, Ghsi111_H, gsi111_T, gsi111_B, and gsi111_H represent graphene on hydrogenated Si (111) and clean Si (111) surfaces of T, B, and H arrangement, respectively. Ghsi100 and gsi100 represent graphene on hydrogenated Si (100) and clean Si (100) surfaces, respectively. Gray, yellow, and white balls represent C, Si, and H atoms, respectively. The Fermi energy is indicated by the dashed line. The value of the band gap is highlighted in each figure in units of "meV".

TABLE 1. Average Distance *d* (Å), Adsorption Energy Δ*E* (meV/Graphene Unit), and Band Gap (meV) of Monolayer Graphene Adsorbed on Different Si Surfaces

	hydrogenated Si(111)			clean Si(111)		
adsorption site	*d*	Δ*E*	band gap	*d*	Δ*E*	band gap
top	2.51	−37.0	0	2.26	−119.8	81.6
bridge	2.51	−37.2	20	2.22	−123.9	272.1
hollow	2.49	−37.2	18	2.23	−123.9	217.7
	clean Si(100)			hydrogenated Si(100)		
	2.54	−32.6	108.8	2.27	−58.5	0

surface is reconstructed, the symmetry of graphene is broken more substantively, leading to a significant band gap of 108 meV.

On the other hand, on clean Si surfaces, strong interactions between Si and C atoms significantly modify the linear bands near the Dirac point of graphene. See Figure 1e−h. The electronic characteristics of graphene disappear completely. For example, Figure 1h shows the band structure of gsi100 is metallic. The bands of Si predominantly near the Fermi level for the gsi100 system indicate there are evident localized surface states in the band structure, which arise from the unsaturated surface Si atoms. In comparison, for clean Si (111) surfaces (Figure 1e, f, g), local surface states near the Fermi level are obviously reduced. This can be explained by the percentage of saturated Si atoms on the Si (111) surface or Si (100) surface. When graphene is adsorbed onto the clean Si (111) surface, all surface Si atoms are saturated by C atoms from graphene, whereas only 50% of Si atoms of the Si 100 surface are saturated by C atoms from graphene.

For monolayer graphene on the clean Si (111) surface, graphene forms bonds with Si atoms, part of the C atoms of graphene change from sp^2 to sp^3, and the band gap deviates from the gamma point. As the symmetry of graphene is broken, the band gaps change to 81.6, 272.1, and 217.7 meV for gsi111_T, gsi111_B, and gsi111_H, respectively. Note that the value of 272.1 meV is the largest band gap ever reported for graphene; in comparison, the gap of graphene adsorbed on SiO_2, SiC, and BN surfaces is

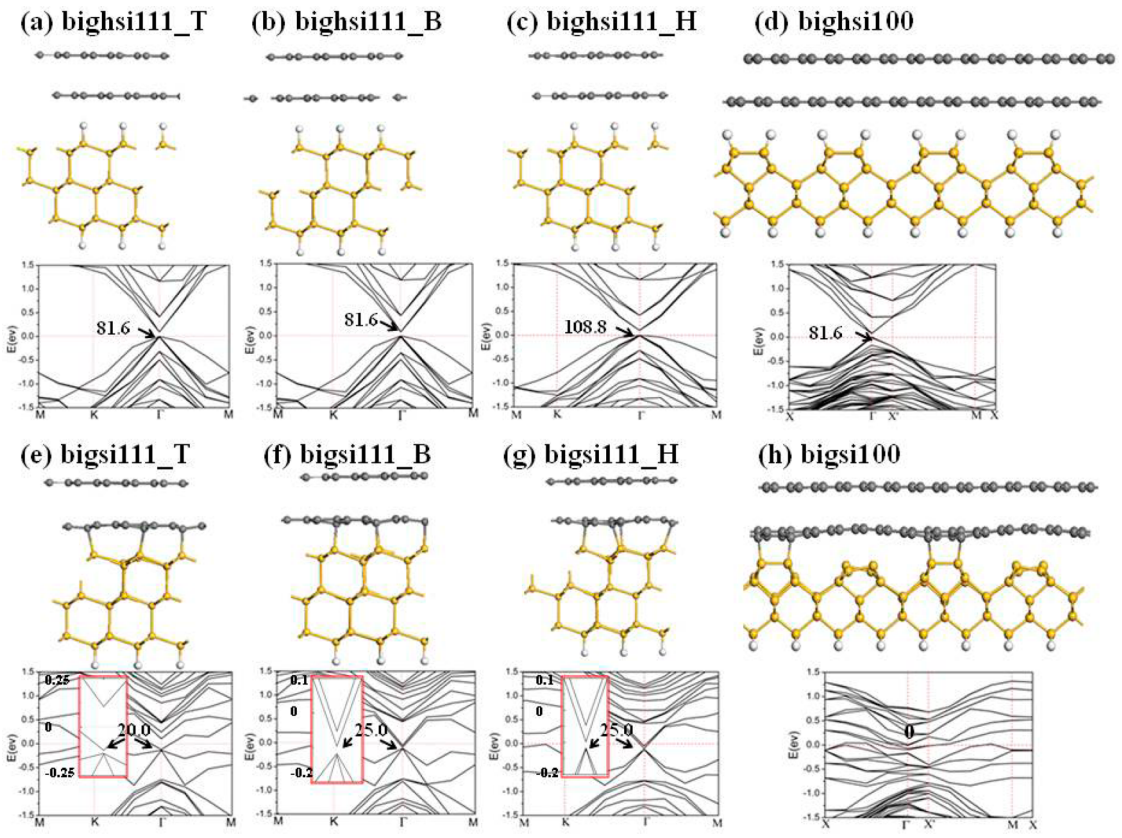

Figure 2. Bilayer graphene on different silicon surfaces and the corresponding band structures. (a) bighsi111_T, (b) bighsi111_B, (c) bighsi111_H, (d) bighsi100, (e) bigsi111_T, (f) bigsi111_B, (g) bigsi111_H, (h) bigsi100. "bighsi111_T" represents a bilayer-graphene-hydrogen-silicon-111 surface with T configuration. The definition of T configuration, B configuration, and H configuration is in Figure S1 of the Supporting Information. Bighsi111_T, bighsi111_B, bighsi111_H, bigsi111_T, bigsi111_B, and bigsi111_H represent bilayer graphene on hydrogenated Si (111) and clean Si (111) surfaces with T, B, or H configuration. Bighsi100 and bigsi100 represent bilayer graphene on hydrogenated Si (100) and clean Si (100) surfaces, respectively. Gray, yellow, and white balls represent C, Si, and H atoms, respectively. The Fermi energy is indicated by the dashed line. Their first Brillouin zones are the same as the monolayer system as shown in Figure S2.

130,[33] 260,[9] and 126 meV,[46] respectively. The gap values are significantly higher than k_BT at room temperature, indicating the achievable current on/off ratio is larger than that of the freestanding graphene.

The corresponding different charge density isosurfaces are shown in Figure S3 of the Supporting Information. Different charge density is defined as

$$\Delta n(r) = n_{\text{total}}(r) - n_{\text{graphene}}(r) - n_{\text{Si}}(r)$$

Figure S3a–d clearly indicates the absence of covalent bonding between C and hydrogenated Si atoms. Since the Si dangling bonds are passivated by H atoms, the interaction between C and Si atoms is dominated by van der Waals forces. Figure S3e–h suggests a strong interaction between graphene and clean silicon surface. Electrons within the common energy levels are shared between the bonded graphene and Si surface atoms. The Mulliken charges[47] on the Si atoms of the C–Si bonds range from 0.26 to 0.32 *e*, whereas the Mulliken charges on C atoms of the C–Si bonds range from −0.45 to −0.47 *e*. The charge redistribution at the graphene–Si interface is the result of electron transfer between the graphene and Si. As surface-state electrons transfer from the Si surface to the graphene monolayer, the graphene becomes n-doped and negatively charged. The findings are similar to those for monolayer graphene on a SiC surface.[28] Thus, a p–n junction is formed between the n-type graphene and p-type Si substrate.

Bilayer Graphene on a Si Surface. In 2006, an approach for opening the band gap in bilayer graphene was proposed[48] in the presence of a potential between the layers, while the electronic properties of bilayer graphene on a SiO_2 surface were investigated by Cuong *et al.* in 2011.[34] Here we investigate bilayer graphene adsorbed on clean or hydrogenated Si surfaces.

Our results show that the strength of the interaction between the two layers of graphene is weak, similar to that in the bulk graphite. In our study, two layers of graphene (*AB* stacking) are placed onto the Si surface. The distance between the graphene layers is 3.35 Å for hydrogenated Si (111) _T, 3.34 Å for hydrogenated Si (111) _B, 3.35 Å for hydrogenated Si (111) _H, 3.31 Å for hydrogenated Si (100), 3.32 Å for clean Si (111) _T, 3.36 Å for clean Si (111) _B, 3.32 Å for clean Si (111) _H, and

TABLE 2. Band Gap (meV) of Graphene Adsorbed on Different Si Surfaces

	hydrogenated Si (111)		clean Si (111)	
adsorption site	monolayer	bilayer	monolayer	bilayer
top	0	81.6	81.6	20
bridge	20	81.6	272.1	25
hollow	18	108.8	217.7	25
	hydrogenated Si (100)		clean Si (100)	
	108.8	81.6	0	0

3.38 Å for clean Si (100), while the distance is 3.35 Å in the bulk graphite.

Due to weak interlayer interactions, the upper layer of graphene maintains the planar geometry as show in Figure 2. When bilayer graphenes are adsorbed onto different Si surfaces, they show similar band gaps. The band gaps are summarized in Figure 2 and Table 2. The band gaps of bighsi111_T, bighsi111_B, bighsi111_H, bighsi100, bigsi111_T, bigsi111_B, bigsi111_H, and bigsi100 are 81.6, 81.6, 108.8, 81.6, 20.0, 25.0, 25.0, and 0 meV, respectively. The different charge density isosurfaces for the bilayer graphene adsorbed onto a Si surface are shown in Figure S4. We obtain similar results in Figure S3 for monolayer graphene adsorbed onto a Si surface.

As shown in Figure 2a–d, bilayer graphenes adsorbed onto hydrogenated Si surfaces lead to bigger band gaps than monolayer graphene adsorbed onto a hydrogenated Si surface. For example, bighsi111_H (Figure 2c) shows a bigger band gap of 108.8 meV than the band gap of 18 meV for ghsi111_H (Figure 1c). In comparison, Figure 2e–h show that bilayer graphenes adsorbed onto a clean Si surface lead to smaller band gaps than monolayer graphenes adsorbed onto a clean Si surface. For example, bigsi111_H (Figure 2g) shows a smaller band gap of 25.0 meV than that of gsi111_H (217.7 meV in Figure 1g).

For bilayer graphenes adsorbed onto a clean Si surface, the upper layer of graphene keeps the structure and band structure of graphene. The inner layer forms chemical bonds with the Si surface and loses the characteristics of graphene. This could be validated by the orbital analysis. As shown in Figures S5 and S6, for bilayer graphenes adsorbed onto a clean Si surface, the HOMO and LUMO orbitals locate on the upper layer of graphene. Thus, the bilayer graphene adsorbed onto a clean Si surface shows a band structure similar to graphene with a small band gap of 0–25 meV (Figure 2). In comparison, monolayer graphene adsorbed onto a clean Si surface loses the graphene characteristics and the band gap is as high as 272 meV (Figure 1).

For bilayer graphene adsorbed onto a hydrogenated Si surface, both the interaction between the two layers of the graphene and that between the inner graphene layer and Si surface are weak. However, as more asymmetry is introduced, typically bilayer graphene adsorbed onto a hydrogenated Si surface shows a larger band gap than monolayer graphene adsorbed. For example, bighsi111_H (Figure 2c) shows a bigger band gap of 108.8 meV than ghsi111_H (18 meV, Figure 1c).

CONCLUSIONS

Using first-principles calculations, we investigate the electronic structures of monolayer and bilayer graphene adsorbed onto clean or H-passivated Si (111)/Si (100) surfaces. The calculations show that the interaction between monolayer graphene and a H-passivated Si surface is weak with a negligible band gap. For bilayer graphene adsorbed onto a H-passivated Si surface, the band gap is opened up to 108 meV due to the introduction of asymmetry. In comparison, the interaction between graphene and a clean Si surface is much stronger, leading to formation of chemical bonds and a large band gap of 272 meV. Our results provide useful information for designing devices by integrating graphene with Si technology.

METHODS

Our calculations of both the optimizations and the electronic structures are performed by the DFT program $DMol_3$ (MS 6.0).[49,50] The interactions between the electrons and ion cores are described by the Perdew–Wang (PWC)[51] functional, and the exchange–correlation energy is described by the local spin density approximation (LSDA). We chose the LSDA because it describes the spacing between the graphene and Si-based substrate better than the generalized gradient approximation functional (GGA). This conforms to the fact that LSDA, despite the lack of long-range nonlocal correlations, produces reasonable interlayer distances in van der Waals crystals such as graphite.[52,53] The semilocal generalized gradient approximation, which violates this balance, fails to generate the interplanar bonding in graphite,[53] while producing a band structure identical to LSDA. The Brillouin zone integration is performed with $5 \times 5 \times 1$ and $1 \times 9 \times 1$ k-point samplings for geometry optimization of Si (111) and Si (100) surfaces, with $11 \times 11 \times 1$ and $1 \times 19 \times 1$ k-point samplings for total energy calculations on Si (111) and Si (100) surfaces, respectively. Our testing results show that these set of parameters are accurate enough to ensure the total energy convergence. First Brillouin zones for Si (111) + graphene and Si (100) + graphene are shown in Figure S2. All the systems are optimized up to the residual force on every atom to be less than 2.0×10^{-3} Ha/Å. The conjugated-gradient minimization scheme is used for both the geometry optimization and electronic structure calculation. To test the reliability of our calculations, the lattice parameter and band gap of bulk Si are calculated by the same settings for comparison. Our calculated lattice parameter of bulk Si (5.42 Å) is close to the experimentally measured value (5.43 Å).[54] The calculated band gap of bulk Si is 0.74 eV, indicating that the LSDA underestimates the band gap (the experimental value is 1.17 eV[55]). However, the calculated value is comparable to the previously reported E_g of bulk Si by GGA, which ranges from 0.59 to 0.79 eV.[56–59]

Conflict of Interest: The authors declare no competing financial interest.

Supporting Information Available: The Supporting Information is available free of charge on the ACS Publications website at DOI: 10.1021/acsnano.5b03722.

Descriptions of the computational models, the first Brillouin zones, the charge density of gsi and frontier molecular orbitals (HOMO and LUMO) on bighsi (PDF)

Acknowledgment. The work is supported by the National Basic Research Program of China (973 Program, Grant No. 2012CB932400), the National Natural Science Foundation of China (Grant Nos. 91233115, 21273158, and 91227201), and a Project Funded by the Priority Academic Program Development of Jiangsu Higher Education Institutions (PAPD). This is also a project supported by the Fund for Innovative Research Teams of Jiangsu Higher Education Institutions, Jiangsu Key Laboratory for Carbon-Based Functional Materials and Devices, Collaborative Innovation Center of Suzhou Nano Science and Technology.

REFERENCES AND NOTES

1. Geim, A. K.; Novoselov, K. S. The Rise of Graphene. *Nat. Mater.* **2007**, *6*, 183–191.
2. Lu, G. H.; Yu, K. H.; Wen, Z. H.; Chen, J. H. Semiconducting Graphene: Converting Graphene from Semimetal to Semiconductor. *Nanoscale* **2013**, *5*, 1353–1368.
3. Wong, S. L.; Huang, H.; Wang, Y.; Cao, L.; Qi, D.; Santoso, I.; Chen, W.; Wee, A. T. S. Quasi-free-standing Epitaxial Graphene on SiC (0001) by Fluorine Intercalation from a Molecular Source. *ACS Nano* **2011**, *5*, 7662–7668.
4. Natan, A.; Hersam, M. C.; Seideman, T. Insights into Graphene Functionalization by Single Atom Doping. *Nanotechnology* **2013**, *24*, 505715.
5. Huang, L.; Pan, Y.; Pan, L.; Gao, M.; Xu, W.; Que, Y.; Zhou, H.; Wang, Y.; Du, S.; Gao, H.-J. Intercalation of Metal Islands and Films at the Interface of Epitaxially Grown Graphene and Ru (0001) Surfaces. *Appl. Phys. Lett.* **2011**, *99*, 163107.
6. Walter, A. L.; Jeon, K.-J.; Bostwick, A.; Speck, F.; Ostler, M.; Seyller, T.; Moreschini, L.; Kim, Y. S.; Chang, Y. J.; Horn, K. Highly p-Doped Epitaxial Graphene Obtained by Fluorine Intercalation. *Appl. Phys. Lett.* **2011**, *98*, 184102.
7. Sutter, P.; Sadowski, J. T.; Sutter, E. A. Chemistry under Cover: Tuning Metal– Graphene Interaction by Reactive Intercalation. *J. Am. Chem. Soc.* **2010**, *132*, 8175–8179.
8. Oostinga, J. B.; Heersche, H. B.; Liu, X.; Morpurgo, A. F.; Vandersypen, L. M. Gate-Induced Insulating State in Bilayer Graphene Devices. *Nat. Mater.* **2008**, *7*, 151–157.
9. Zhou, S.; Gweon, G.-H.; Fedorov, A.; First, P.; De Heer, W.; Lee, D.-H.; Guinea, F.; Neto, A. C.; Lanzara, A. Substrate-Induced Bandgap Opening in Epitaxial Graphene. *Nat. Mater.* **2007**, *6*, 770–775.
10. Craciun, M.; Russo, S.; Yamamoto, M.; Oostinga, J. B.; Morpurgo, A.; Tarucha, S. Trilayer Graphene Is a Semimetal with a Gate-Tunable Band Overlap. *Nat. Nanotechnol.* **2009**, *4*, 383–388.
11. Jin, L.; Fu, Q.; Mu, R.; Tan, D.; Bao, X. Pb Intercalation Underneath a Graphene Layer on Ru (0001) and Its Effect on Graphene Oxidation. *Phys. Chem. Chem. Phys.* **2011**, *13*, 16655–16660.
12. Nagashima, A.; Tejima, N.; Oshima, C. Electronic States of the Pristine and Alkali-Metal-Intercalated Monolayer Graphite/Ni (111) Systems. *Phys. Rev. B: Condens. Matter Mater. Phys.* **1994**, *50*, 17487.
13. Virojanadara, C.; Watcharinyanon, S.; Zakharov, A.; Johansson, L. I. Epitaxial Graphene on 6 H-SiC and Li Intercalation. *Phys. Rev. B: Condens. Matter Mater. Phys.* **2010**, *82*, 205402.
14. Riedl, C.; Coletti, C.; Iwasaki, T.; Zakharov, A.; Starke, U. Quasi-Free-Standing Epitaxial Graphene on SiC Obtained by Hydrogen Intercalation. *Phys. Rev. Lett.* **2009**, *103*, 246804.
15. Varykhalov, A.; Sánchez-Barriga, J.; Shikin, A.; Biswas, C.; Vescovo, E.; Rybkin, A.; Marchenko, D.; Rader, O. Electronic and Magnetic Properties of Quasifreestanding Graphene on Ni. *Phys. Rev. Lett.* **2008**, *101*, 157601.
16. Kosynkin, D. V.; Higginbotham, A. L.; Sinitskii, A.; Lomeda, J. R.; Dimiev, A.; Price, B. K.; Tour, J. M. Longitudinal Unzipping of Carbon Nanotubes to Form Graphene Nanoribbons. *Nature* **2009**, *458*, 872–876.
17. Barone, V.; Peralta, J. E. Magnetic Boron Nitride Nanoribbons with Tunable Electronic Properties. *Nano Lett.* **2008**, *8*, 2210–2214.
18. Ritter, K. A.; Lyding, J. W. The Influence of Edge Structure on the Electronic Properties of Graphene Quantum Dots and Nanoribbons. *Nat. Mater.* **2009**, *8*, 235–242.
19. Son, Y.-W.; Cohen, M. L.; Louie, S. G. Energy Gaps in Graphene Nanoribbons. *Phys. Rev. Lett.* **2006**, *97*, 216803.
20. Yang, L.; Park, C.-H.; Son, Y.-W.; Cohen, M. L.; Louie, S. G. Quasiparticle Energies and Band Gaps in Graphene Nanoribbons. *Phys. Rev. Lett.* **2007**, *99*, 186801.
21. Boukhvalov, D.; Katsnelson, M. Destruction of Graphene by Metal Adatoms. *Appl. Phys. Lett.* **2009**, *95*, 023109.
22. Premlal, B.; Cranney, M.; Vonau, F.; Aubel, D.; Casterman, D.; De Souza, M.; Simon, L. Surface Intercalation of Gold Underneath a Graphene Monolayer on SiC (0001) Studied by Scanning Tunneling Microscopy and Spectroscopy. *Appl. Phys. Lett.* **2009**, *94*, 263115.
23. Velasco, J. M.; Kelaidis, N.; Xenogiannopoulou, E.; Raptis, Y.; Tsoutsou, D.; Tsipas, P.; Speliotis, T.; Pilatos, G.; Likodimos, V.; Falaras, P. Electronic Band Structure Imaging of Three Layer Twisted Graphene on Single Crystal Cu (111). *Appl. Phys. Lett.* **2013**, *103*, 213108.
24. Gierz, I.; Suzuki, T.; Weitz, R. T.; Lee, D. S.; Krauss, B.; Riedl, C.; Starke, U.; Höchst, H.; Smet, J. H.; Ast, C. R. Electronic Decoupling of an Epitaxial Graphene Monolayer by Gold Intercalation. *Phys. Rev. B: Condens. Matter Mater. Phys.* **2010**, *81*, 235408.
25. Cheng, Y.; Schwingenschlögl, U. A Route to Strong p-Doping of Epitaxial Graphene on SiC. *Appl. Phys. Lett.* **2010**, *97*, 193304.
26. Ruan, M.; Hu, Y.; Guo, Z.; Dong, R.; Palmer, J.; Hankinson, J.; Berger, C.; De Heer, W. A. Epitaxial Graphene on Silicon Carbide: Introduction to Structured Graphene. *MRS Bull.* **2012**, *37*, 1138–1147.
27. Ohta, T.; El Gabaly, F.; Bostwick, A.; McChesney, J. L.; Emtsev, K. V.; Schmid, A. K.; Seyller, T.; Horn, K.; Rotenberg, E. Morphology of Graphene Thin Film Growth on SiC (0001). *New J. Phys.* **2008**, *10*, 023034.
28. Varchon, F.; Feng, R.; Hass, J.; Li, X.; Nguyen, B. N.; Naud, C.; Mallet, P.; Veuillen, J.-Y.; Berger, C.; Conrad, E. H. Electronic Structure of Epitaxial Graphene Layers on SiC: Effect of the Substrate. *Phys. Rev. Lett.* **2007**, *99*, 126805.
29. Giovannetti, G.; Khomyakov, P. A.; Brocks, G.; Kelly, P. J.; van den Brink, J. Substrate-Induced Band Gap in Graphene on Hexagonal Boron Nitride: Ab Initio Density Functional Calculations. *Phys. Rev. B: Condens. Matter Mater. Phys.* **2007**, *76*, 073103.
30. Joshi, N.; Ghosh, P. Substrate-Induced Changes in the Magnetic and Electronic Properties of Hexagonal Boron Nitride. *Phys. Rev. B: Condens. Matter Mater. Phys.* **2013**, *87*, 235440.
31. Sławińska, J.; Zasada, I.; Klusek, Z. Energy Gap Tuning in Graphene on Hexagonal Boron Nitride Bilayer System. *Phys. Rev. B: Condens. Matter Mater. Phys.* **2010**, *81*, 155433.
32. Lari, L.; Hughes, G.; Muramoto, K.; Hirohata, A.; Shiraishi, M.; Lazarov, V. In *Correlation of Microstructure and Transport Properties of Multilayered Graphene Spin Valves on SiO_2/Si*; Journal of Physics: Conference Series, IOP Publishing, 2013; p 012048.
33. Kang, Y.-J.; Kang, J.; Chang, K. Electronic Structure of Graphene and Doping Effect on SiO2. *Phys. Rev. B: Condens. Matter Mater. Phys.* **2008**, *78*, 115404.
34. Nguyen, T. C.; Otani, M.; Okada, S. Semiconducting Electronic Property of Graphene Adsorbed on (0001) Surfaces of SiO2. *Phys. Rev. Lett.* **2011**, *106*, 106801.
35. Lahiri, J.; Miller, T.; Adamska, L.; Oleynik, I. I.; Batzill, M. Graphene Growth on Ni (111) by Transformation of a Surface Carbide. *Nano Lett.* **2011**, *11*, 518–522.

36. Fuentes-Cabrera, M.; Baskes, M. I.; Melechko, A. V.; Simpson, M. L. Bridge Structure for the Graphene/Ni (111) System: a First Principles Study. *Phys. Rev. B: Condens. Matter Mater. Phys.* **2008**, *77*, 035405.
37. Nobis, D.; Potenz, M.; Niesner, D.; Fauster, T. Image-Potential States of Graphene on Noble-Metal Surfaces. *Phys. Rev. B: Condens. Matter Mater. Phys.* **2013**, *88*, 195435.
38. Gamo, Y.; Nagashima, A.; Wakabayashi, M.; Terai, M.; Oshima, C. Atomic Structure of Monolayer Graphite Formed on Ni (111). *Surf. Sci.* **1997**, *374*, 61–64.
39. Ohta, T.; Bostwick, A.; Seyller, T.; Horn, K.; Rotenberg, E. Controlling the Electronic Structure of Bilayer Graphene. *Science* **2006**, *313*, 951–954.
40. Zhang, Y.; Tang, T.-T.; Girit, C.; Hao, Z.; Martin, M. C.; Zettl, A.; Crommie, M. F.; Shen, Y. R.; Wang, F. Direct Observation of a Widely Tunable Bandgap in Bilayer Graphene. *Nature* **2009**, *459*, 820–823.
41. Castro, E. V.; Novoselov, K.; Morozov, S.; Peres, N.; Dos Santos, J. L.; Nilsson, J.; Guinea, F.; Geim, A.; Neto, A. C. Biased Bilayer Graphene: Semiconductor with a Gap Tunable by the Electric Field Effect. *Phys. Rev. Lett.* **2007**, *99*, 216802.
42. Hackley, J.; Ali, D.; DiPasquale, J.; Demaree, J.; Richardson, C. Graphitic Carbon Growth on Si (111) Using Solid Source Molecular Beam Epitaxy. *Appl. Phys. Lett.* **2009**, *95*, 133114.
43. Xu, Y.; He, K.; Schmucker, S.; Guo, Z.; Koepke, J.; Wood, J.; Lyding, J.; Aluru, N. Inducing Electronic Changes in Graphene Through Silicon (100) Substrate Modification. *Nano Lett.* **2011**, *11*, 2735–2742.
44. Moon, J.; Curtis, D.; Bui, S.; Marshall, T.; Wheeler, D.; Valles, I.; Kim, S.; Wang, E.; Weng, X.; Fanton, M. Top-Gated Graphene Field-Effect Transistors Using Graphene on Si (111) Wafers. *IEEE Electron Device Lett.* **2010**, *31*, 1193–1195.
45. Tayran, C.; Zhu, Z.; Baldoni, M.; Selli, D.; Seifert, G.; Tománek, D. Optimizing Electronic Structure and Quantum Transport at the Graphene-Si (111) Interface: An Ab Initio Density-Functional Study. *Phys. Rev. Lett.* **2013**, *110*, 176805.
46. Shinde, P. P.; Kumar, V. Direct Band Gap Opening in Graphene by BN Doping: Ab Initio Calculations. *Phys. Rev. B: Condens. Matter Mater. Phys.* **2011**, *84*, 125401.
47. Mulliken, R. S. Electronic Population Analysis on LCAO-MO Molecular Wave Functions. II. Overlap Populations, Bond Orders, and Covalent Bond Energies. *J. Chem. Phys.* **1955**, *23*, 1841–1846.
48. McCann, E. Asymmetry Gap in the Electronic Band Structure of Bilayer Graphene. *Phys. Rev. B: Condens. Matter Mater. Phys.* **2006**, *74*, 161403.
49. Delley, B. From Molecules to Solids with the DMol3 Approach. *J. Chem. Phys.* **2000**, *113*, 7756–7764.
50. Delley, B. Fast Calculation of Electrostatics in Crystals and Large Molecules. *J. Phys. Chem.* **1996**, *100*, 6107–6110.
51. Perdew, J. P.; Wang, Y. Accurate and Simple Analytic Representation of the Electron-Gas Correlation Energy. *Phys. Rev. B: Condens. Matter Mater. Phys.* **1992**, *45*, 13244–13249.
52. Charlier, J.-C.; Gonze, X.; Michenaud, J.-P. Graphite Interplanar Bonding: Electronic Delocalization and van der Waals Interaction. *EPL (Europhysics Letters)* **1994**, *28*, 403.
53. Ooi, N.; Rairkar, A.; Adams, J. B. Density Functional Study of Graphite Bulk and Surface Properties. *Carbon* **2006**, *44*, 231–242.
54. Okada, Y.; Tokumaru, Y. Precise Determination of Lattice Parameter and Thermal Expansion Coefficient of Silicon between 300 and 1500 K. *J. Appl. Phys.* **1984**, *56*, 314–320.
55. Persson, C.; Lindefelt, U. Detailed Band Structure for 3C-, 2H-, 4H-, 6H-SiC, and Si around the Fundamental Band Gap. *Phys. Rev. B: Condens. Matter Mater. Phys.* **1996**, *54*, 10257–10260.
56. Ng, M.-F.; Zhou, L.; Yang, S.-W.; Sim, L. Y.; Tan, V. B. C.; Wu, P. Theoretical Investigation of Silicon Nanowires: Methodology, Geometry, Surface Modification, and Electrical Conductivity Using a Multiscale Approach. *Phys. Rev. B: Condens. Matter Mater. Phys.* **2007**, *76*, 155435.
57. Leu, P. W.; Svizhenko, A.; Cho, K. Ab Initio Calculations of the Mechanical and Electronic Properties of Strained Si Nanowires. *Phys. Rev. B: Condens. Matter Mater. Phys.* **2008**, *77*, 235305.
58. Heyd, J.; Peralta, J. E.; Scuseria, G. E.; Martin, R. L. Energy Band Gaps and Lattice Parameters Evaluated with the Heyd-Scuseria-Ernzerhof Screened Hybrid Functional. *J. Chem. Phys.* **2005**, *123*, 174101.
59. Zhang, R. Q.; Zheng, W. T.; Jiang, Q. External Electric Field Modulated Electronic and Structural Properties of <111> Si Nanowires. *J. Phys. Chem. C* **2009**, *113*, 10384–10389.